Amita Bedar, Beena G. Singh, Pradip K. Tewari, Ramesh C. Bindal and Soumitra Kar*

# Kinetics studies on free radical scavenging property of ceria in polysulfone–ceria radiation resistant mixed-matrix membrane

https://doi.org/10.1515/ijcre-2020-0123
Received July 30, 2020; accepted March 11, 2021;
published online March 24, 2021

**Abstract:** Cerium oxide (ceria) contains two stable states of cerium ions ($Ce^{3+}$ and $Ce^{4+}$). The presence of these two states and the ability to swap from one state to another ($Ce^{3+} \leftrightarrow Ce^{4+}$) by scavenging the highly reactive oxygen species (ROS) generated from radiolysis of water, ensure the enhanced stability of polysulfone (Psf) membranes in the γ-radiation environment. In this study, the ROS scavenging ability of ceria was studied. Ceria nanoparticles were found to scavenge ROS like hydroxyl radicals and hydrogen peroxide ($H_2O_2$). The $H_2O_2$ scavenging is due to the peroxidase-like catalytic activity of ceria nanoparticles. The ROS scavenging is responsible for offering protection to the Psf host matrix and in turn the stability to the Psf-ceria mixed-matrix membranes (MMMs) in γ-radiation environment. Thus, presence of ceria nanoparticles provides an opportunity for utilizing Psf-ceria MMMs in ionizing radiation environment with increased life span, without compromise in the performance.

**Keywords:** ceria nanoparticles; hydroxyl radical scavenging; membrane; peroxidase-like activity; polysulfone; γ-radiation.

## 1 Introduction

The rapid technological and industrial development has brought attention towards rare earth materials, also known as 'industrial vitamins' and a 'treasury' of new materials (Hu et al. 2006). The rare earth elements have a different chemistry from other elements from main group and transition metals due to the characteristic property of their 4*f* orbitals. The 4*f* orbitals are guarded from the atom's environment by 4*d* and 5*p* electrons (Bouzigues, Gacoin, and Alexandrou 2011; Hu et al. 2006) as they are enfolded inside the atom. Rare earth materials have distinctive catalytic, magnetic and electronic properties due to these 4*f* orbitals. These unique properties have been utilized to accomplish newer applications in various industrial technologies such as information and biotechnology (Bouzigues, Gacoin, and Alexandrou 2011), which are not feasible with the transition and main group metals.

The first element in the lanthanide group, cerium (Ce) has significant application potential in the areas of chemistry, physics, biology, and material science. Ce along with oxygen can develop nanoparticles in the form of cerium oxide, carrying a fluorite crystalline structure, which came out as a thought-provoking material (Conesa 1995) to researchers. It has been used for inventive applications such as oxidation protection materials at high-temperature (Patil et al. 2002), catalytic materials (Kašpar, Fornasiero, and Graziani 1999; Trovarelli 1996), fuel cells (Stambouli and Traversa 2002), solar cells (Corma et al. 2004), pharmacological agents (Celardo et al. 2011), gas sensor (Beie and Gnörich 1991; Izu, Shin, and Murayama 2003; Jasinski, Suzuki, and Anderson 2003; Stefanik and Tuller 2001), and optical glass polishing (Belkhir, Bouzid, and Herold 2009; Wang et al. 2007).

The lanthanide series elements generally exist in the trivalent (+3) state. Interestingly, due to the presence of two partially occupied subshells of electron, cerium atoms exhibit either fully reduced (+3) state or fully oxidized (+4) state. Therefore, oxide of cerium (cerium oxide or ceria) plays a dual character, as a reducing as well as oxidizing component. These phenomena occur due to the feasible swapping between $Ce^{4+}$ and $Ce^{3+}$ (Cafun et al. 2013; Goris et al. 2014; Li et al 2009; Wang et al 2015; Zhang et al. 2004). The vacancy of oxygen gets created, transferred, and eliminated, along with the cerium atom (Esch et al. 2005). This property improves adsorption of reactive oxygen radicals (Bosnjakovic and Schlick 2004; Fernandez-Garcia et al.

***Corresponding author: Soumitra Kar**, Homi Bhabha National Institute, Mumbai 400094, India; and Membrane Development Section, Bhabha Atomic Research Centre, Mumbai 400085, India, E-mail: soumitra.1stmay@gmail.com.
https://orcid.org/0000-0002-4766-9903
**Amita Bedar and Ramesh C. Bindal,** Homi Bhabha National Institute, Mumbai 400094, India; and Membrane Development Section, Bhabha Atomic Research Centre, Mumbai 400085, India
**Beena G. Singh,** Homi Bhabha National Institute, Mumbai 400094, India; and Radiation & Photochemistry Division, Bhabha Atomic Research Centre, Mumbai 400085, India
**Pradip K. Tewari,** Homi Bhabha National Institute, Mumbai 400094, India

2016; Schlick et al. 2016; Yang and Gao 2006) and promotes electron transfer (Campbell and Peden 2005). Oxygen vacancies generate on the reduction of $Ce^{4+}$ to $Ce^{3+}$, which can be described by the Kroger–Vink notation (Anandkumar et al. 2015), as shown in Eq. (1).

$$O_O^X + 2Ce_{Ce}^X \leftrightarrow V_O^{\bullet\bullet} + 2Ce'_{Ce} + \frac{1}{2}O_2 \quad (1)$$

where, $O_O^X$ is a neutral oxygen on an oxygen lattice site and $Ce_{Ce}^X$ is a neutral cerium on a neutral cerium site, $V_O^{\bullet\bullet}$ is a +2 oxygen vacancy and $Ce'_{Ce}$ is a $Ce^{3+}$ atom in a $Ce^{4+}$ site giving it a net negative charge of –1.

The valence switching ability between $Ce^{3+}$ and $Ce^{4+}$ provides the free radical scavenging capability as well as catalytic activity of ceria nanoparticles.

The hydroxyl free radial ($^{\bullet}OH$) is a highly reactive one that could be scavenged by the ceria nanoparticles through conversion from $Ce^{3+}$ to $Ce^{4+}$, as shown in Eq. (2) (Xu and Qu 2014).

$$Ce_2O_3 + 2[^{\bullet}OH] \rightarrow 2CeO_2 + H_2O \quad (2)$$

It can be regenerated as shown in Eq. (3).

$$2CeO_2 \xrightarrow{H^+(aq)} Ce_2O_3 + \frac{1}{2}O_2 \quad (3)$$

Peroxidase are capable to catalyze the reduction of peroxide in presence of certain co-factors, as shown in Eq. (4) (Vinothkumar et al. 2018).

$$ROOR' + 2e^- + 2H^+ \rightarrow ROH + R'OH \quad (4)$$

Several nanomaterials are (Liu et al. 2019; Mu et al. 2012, 2018; Zhao et al. 2015) found to have peroxidase-like activity similar to the mechanism of Fenton reaction. Cerium ion can also perform peroxidase-like activity, as shown in Eqs. (5)–(7).

$$Ce^{3+} + H_2O_2 + H^+ \rightarrow Ce^{4+} + OH^{\bullet} + H_2O \quad (5)$$

$$OH^{\bullet} + H_2O_2 \rightarrow HO_2^- + H_2O \quad (6)$$

$$Ce^{4+} + HO_2^- \rightarrow O_2 + Ce^{3+} + H^+ \quad (7)$$

These distinctive properties of ceria nanoparticles are utilized by the authors' group to enhance the radiation stability of polymeric membranes for the application in the treatment of radioactive effluent (Bedar et al. 2019). Polymers, such as polysulfone (Psf), are frequently used materials for membrane fabrication (Ng et al. 2013), but they undergo oxidative degradation on exposure to γ-radiation environment (Bedar et al. 2020). Free radicals generated by γ-ray irradiation leads to chain scissioning and/or crosslinking, and alter the polymer crosslink density (Brown and O'Donnell 1975; Hegazy et al. 1992; Murakami and Kudo 2007). This affects the membrane performance (Rupiasih and Vidyasagar 2008). Impregnation of ceria in the Psf membrane matrix helps to protect the matrix by scavenging free radicals ($^{\bullet}OH$, $e^-_{aq}$, $H_2O_2$, H, $H_2$, $H_3O^+$) generated due to the water radiolysis under γ-radiation (Wu et al. 2018; Zhang et al. 2020). Oxygen reacts with hydrated electron with a rate constant of $1.1 \times 10^{10}\ M^{-1}\ s^{-1}$ at room temperature. Therefore, under the operating environment, the presence of oxygen scavenges the $e^-_{aq}$ efficiently to form the superoxide anion, which slowly dismutase to $H_2O_2$ (Challenger et al. 1996). Therefore, the main oxidants that are detrimental to the membrane stability are hydroxyl radical and hydrogen peroxide.

Presence of the oxygen vacancies on the surface of ceria provides the stable adsorption site and strong affinity (Mullins 2015). The thermodynamics between the polymer matrix and the cerium oxide nanoparticles, through the intrinsic and extrinsic interfacial regions, plays a vital role in ensuring the homogeneous dispersion of cerium oxide nanoparticles in the host and thus can lead to an enhanced-performance composite with synergistic effects (Schadler 2018).

In this study, the ability of ceria nanoparticles to scavenge the oxidizing species and their effect on increasing the stability of the Psf membrane in the radiation environment has been evaluated. Interestingly, Psf-ceria mixed-matrix membranes (MMMs) with the loading of ceria was found to stable due to the scavenging of $^{\bullet}OH$ radical and peroxidase-like activity of ceria nanoparticles.

# 2 Materials and methods

## 2.1 Materials

Cerium nitrate ($Ce(NO_3)_3{\cdot}6H_2O$, AR-grade, purity > 99.9%) was purchased from Indian Rare Earth Limited, India and citric acid ($C_6H_8O_7{\cdot}H_2O$ purity > 99%) was obtained from Merck, India. Polysulfone (Psf, Molecular weight ~ 60 kDa) was procured from Solvay Specialties India Pvt. Ltd, India. N-methyl-2-pyrrolidone (NMP, assay ≥ 99.5%) and AR grade polyvinyl pyrrolidone (PVP, K-30; molecular weight: 40 kDa) were purchased from SRL Pvt. Ltd (Mumbai, India). Malachite green (MG),

ferrous sulfate ($FeSO_4 \cdot 7H_2O$) were obtained from Sigma-Aldrich. Hydrogen peroxide ($H_2O_2$, 30%) was procured from Merck, India.

### 2.2 Synthesis of ceria nanoparticles

Gel-combustion route was applied to synthesize ceria nanoparticles using cerium nitrate as oxidant and citric acid as fuel. Characterization of ceria nanoparticles was taken place using X-ray diffraction (XRD), X-ray photoelectron spectroscopy (XPS), small angle X-ray scattering (SAXS), transmission electron microscopy (TEM), and energy dispersive X-ray spectroscopy (EDX) techniques. These characterizations ensure the synthesis of pure, crystalline ceria nanoparticles with an average size of 12 nm (Bedar et al 2019).

### 2.3 Synthesis of Psf-ceria MMMs

Phase inversion technique was used to synthesize the Psf-Ceria MMMs, as reported in our previous study (Bedar et al. 2019). In brief, ceria with the different weight fractions (0.1, 0.5, 1, and 2 wt% of Psf) was impregnated in the Psf host membrane matrix having thickness of ~ 200 μm. The membranes are labeled as 0.1-Ce, 0.5-Ce, 1-Ce, and 2-Ce, respectively. Ceria was not added for the synthesis of control Psf membrane. To examine the stability under γ-radiation, control Psf and the MMMs were sealed in a zip-lock bag with de-mineralized water and kept for different doses under γ-radiation in Gamma Chamber (GC-5000, $^{60}Co$ source, Board of Radiation & Isotope Technology, BRIT, India) with ~ 1.5 kGy/h (Fricke dosimetry) dose rate.

### 2.4 Hydroxyl radical scavenging studies

Competition kinetics was performed using MG as reference solute to evaluate $^{\bullet}OH$ radical scavenging activity of the ceria nanoparticles. Hydrogen peroxide was used to oxidize $Fe^{2+}$ ion and generate OH radical by Fenton reaction, shown in Eq. (8) (Babu et al. 2007).

$$Fe^{2+} + H_2O_2 \rightarrow Fe^{3+} + OH^- + OH^{\bullet} \quad (8)$$

A triphenyl methane dye, MG, possesses intense green color, which shows absorption peak at ~ 615 nm. MG instantly reacts with induced $^{\bullet}OH$ radicals and is oxidized (as shown in Eq. (9)), which leads to the decolourization of the dye. The decay of MG was monitored by absorbance at 615 nm with different concentration of ceria nanoparticles as a scavenger.

$$MG + {}^{\bullet}OH \rightarrow MG_{OX} \quad (9)$$

The studies were performed using UV–vis spectrophotometer (JASCO V-630 spectrophotometer) in a quartz cuvette (1 × 1 cm). The reaction mixture contains 12 μM MG, 0.15 mM $FeSO_4$ and varying concentration of ceria nanoparticles or different loading of ceria in MMMs (3 × 1 cm membrane area). Hydrogen peroxide (1 M) was added to initiate reaction. The first order kinetics was used for fitting the absorbance-time plot ($k_{obs}$) in absence and presence of different concentration of ceria, or different loading of ceria in MMMs as scavengers.

### 2.5 Peroxidase activity analysis

Peroxidase-like activity of ceria nanoparticles and Psf-ceria MMMs was investigated by using MG and hydrogen peroxide as substrates. The oxidation of MG by ceria nanoparticles and hydrogen peroxide can be written as in Eq. (10).

$$MG + H_2O_2 \rightarrow MG_{OX} + 2H_2O + O_2 \quad (10)$$

The reaction mixture containing 12 μM MG, 1 M hydrogen peroxide, and varying concentration of ceria nanoparticles was taken up for evaluation of activity. The variation in the absorbance value of different concentration of ceria nanoparticles was determined at the wavelength of 615 nm in the UV–vis spectrophotometer.

Catalytic kinetics of the material was evaluated by employing Lineweaver–Burk plot, using the relation in Eq. (11) (Vinothkumar et al. 2018).

$$\frac{1}{V} = \frac{K_m}{V_{max}}\left(\frac{1}{C} + \frac{1}{K_m}\right) \quad (11)$$

Here, two different sets were used. In first set, in order to evaluate the affinity between the ceria nanoparticles and MG, the reaction was monitored by following the oxidation of MG in presence of fixed concentration of nanoparticles, $H_2O_2$ and varying the concentration of MG. The resulting linear portion of the absorption-time plot at 615 nm was fitted and the slope was divided by the extinction coefficient of MG ($1.4 \times 10^5\ M^{-1}\ cm^{-1}$) to obtain the initial velocity ($V$, M/s). The double reciprocal plot of the initial velocity against the concentration of MG was plotted and the linear fit gave the slope and intercept from where the Michaelis-Menten constant ($K_m$) and maximum initial velocity ($V_{max}$) were calculated. Similarly, the affinity of the nanoparticles towards $H_2O_2$ was evaluated by performing the oxidation of MG in presence of fixed concentration of MG, ceria nanoparticles and varying the concentration of $H_2O_2$. Similarly, this set was evaluated for estimating the kinetic parameter, $K_m$ and $V_{max}$. These parameters were not evaluated for MMMs due to the limitation of the adsorption of the MG on the Psf membrane.

## 3 Results and discussion

### 3.1 X-ray photoelectron spectroscopy of ceria nanoparticles

The XPS spectra of ceria nanoparticles indicate peaks of binding energy at ~881.8, ~897.6, and ~905 eV, which reveal the presence of $Ce^{4+}$, and the peaks at ~887.9, and ~900.9 eV, which reveal the presence of $Ce^{3+}$ (Figure 1). Thus, XPS analyses illustrate the existence of two oxidation states of cerium.

### 3.2 UV–vis spectra of ceria nanoparticles

The UV–vis absorption spectra of ceria nanoparticles are shown in Figure 2. The characteristic absorption peak of $Ce^{3+}$ ion is seen at ~230 nm wavelength, while a broad peak is observed around 300–400 nm, which is attributed to the overlapping of two peaks, absorption of $Ce^{4+}$ (~300 nm) and inter-band charge-transfer transition (~350 nm).

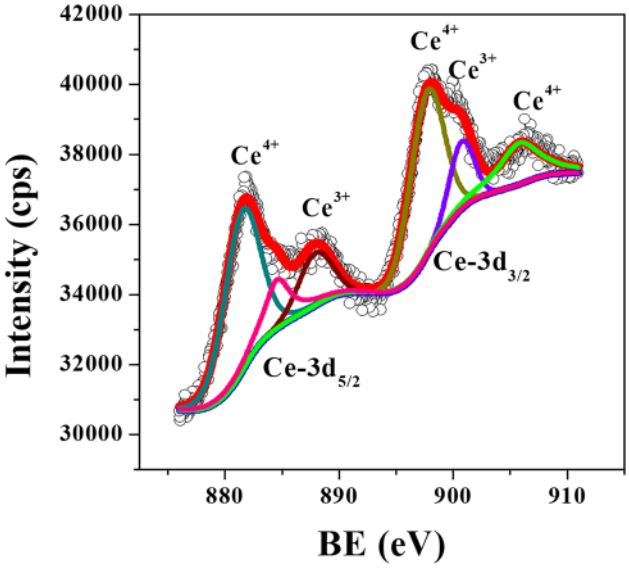


**Figure 1:** X-ray photoelectron spectra of ceria nanoparticles.

Absorption study of ceria nanoparticles confirms the presence of $Ce^{3+}$ and $Ce^{4+}$ ions, as well as the transition phase.

## 3.3 Hydroxyl radical scavenging studies

Hydroxyl radical scavenging activity of ceria nanoparticle in the reaction was evaluated in the presence of different concentration of ceria nanoparticles by determining the decay of MG (at 615 nm absorption peak) due to oxidation by •OH radical, as shown in Figure 3. The inset of Figure 3 shows that the decay of the absorbance due to MG decreases with increase in the concentration of ceria due to •OH radical scavenging capability of ceria nanoparticles. The •OH radical scavenging phenomenon of ceria nanoparticles can be expressed as in Eq. (12).

$$Ce^{3+} + OH^{\bullet} + H^{+} \rightarrow Ce^{4+} + H_2O \quad (12)$$

The decrease in the decay rate of MG ($k_{obs}$) with increasing concentration of ceria indicates that the ceria is scavenging the •OH radical.

Figure 4 shows the MG degradation in the presence of MMMs. Control Psf membrane shows a sudden reduction in the degradation rate of MG. This is due to the rapid reaction of •OH radical with the Psf chains, which causes the degradation of Psf membrane matrix. Degradation of membrane matrix results in the reduction of molecular weight of control Psf membrane under γ-radiation, as shown in our previous work (Bedar et al. 2019). The reaction of •OH radical with organic substrate is non-specific as it reacts with them by three different processes, viz., hydrogen abstraction, •OH radical addition, and one-electron oxidation. The hydrogen abstraction and radical addition processes result in formation of carbon centered radicals, which are known to react rapidly with oxygen and form peroxyl radical. The formation of peroxyl radical are deleterious as they initiate a chain reaction causing formation of more oxidants and thus results in rapid degradation of the polymer. On the other hand, inorganic entity like $Ce^{3+}$ is known to reduce •OH radical to form $Ce^{+4}$ only, which is a relatively stable entity and less deleterious as compared to peroxyl radicals. Thus, loading of the ceria in Psf host matrix gives extra radiation stability to the membrane. Hence the reactivity of •OH radical with Psf-ceria MMMs is reduced.

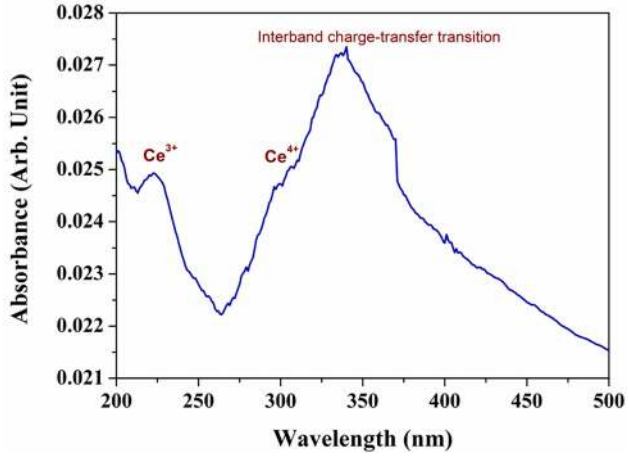


**Figure 2:** UV–vis absorption spectra of ceria nanoparticles.

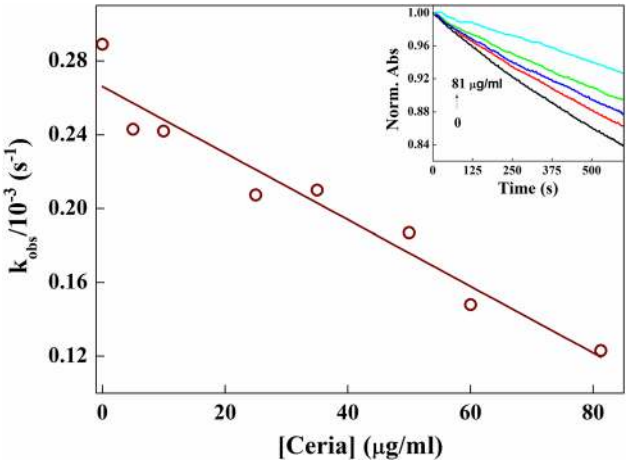


**Figure 3:** Rate of hydroxyl radical scavenging activity by MG in presence of different concentration of ceria nanoparticles (5–81 μg/ml). Inset shows inhibition of absorbance of MG due to •OH radical induced degradation.

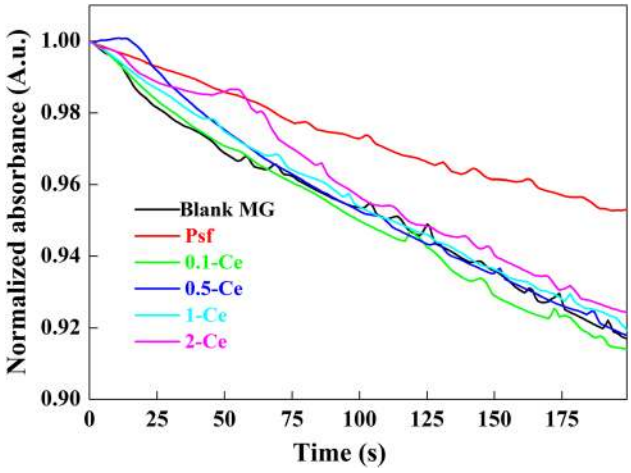


**Figure 4:** Hydroxyl radical reactivity with Psf-ceria MMMs. The inhibition of absorbance of MG due to $^{\bullet}OH$ radical induced degradation in presence of Psf membranes loaded with different concentration of ceria nanoparticles (0.1–2 wt%).

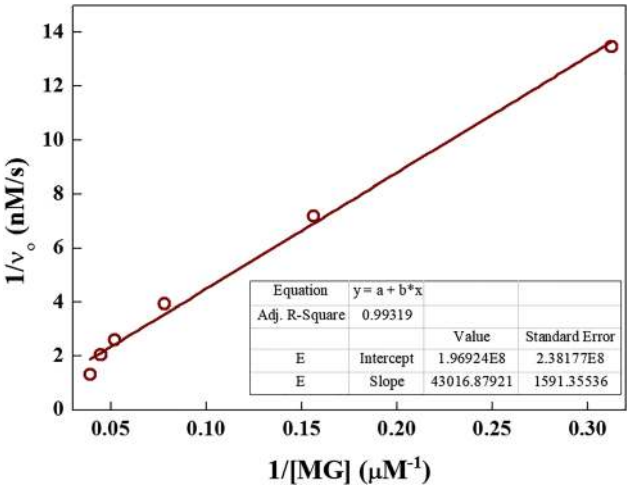


**Figure 6:** Double reciprocal plot of initial velocity for the decay of MG by $H_2O_2$ catalyzed by ceria nanoparticles as a function of MG concentration.

## 3.4 Peroxidase activity analysis

The peroxidase-like activity of ceria nanoparticles was analyzed by using MG and hydrogen peroxide as the substrate. Inset of Figure 5 shows the time dependent peroxidase-like activity of ceria nanoparticles. Peroxidase-like activity is increases with the increasing concentration of ceria nanoparticles (Figure 5). As a result, for the peroxidase activity of Psf-ceria MMMs, the initial velocity was found to increase with ceria loading from 0.418 (blank MG) to 0.461, 0.464, and 0.676 nM/s for control Psf, 0.1-Ce, and 1-Ce MMMs, respectively.

To understand the affinity of MG with ceria nanoparticles, the steady state kinetics was studied by varying the concentration of MG with the fixed concentration of ceria and hydrogen peroxide, as shown in Figure 6. The steady state kinetic parameters were found using Lineweaver–Burke method. The value of $K_m$ was estimated ~ 0.2195 mM and $V_{max}$ ~ 5.1 nM/s. Similarly, to realize the affinity of $H_2O_2$ with ceria nanoparticles, the steady state kinetics was determined by varying concentration of $H_2O_2$ with the fixed concentration of ceria and MG, as shown in Figure 7. The kinetic parameters, $K_m$ and $V_{max}$, are found to be ~ 0.119 M and ~ 82.1 μM/s, respectively. The higher value of $K_m$ indicates the low

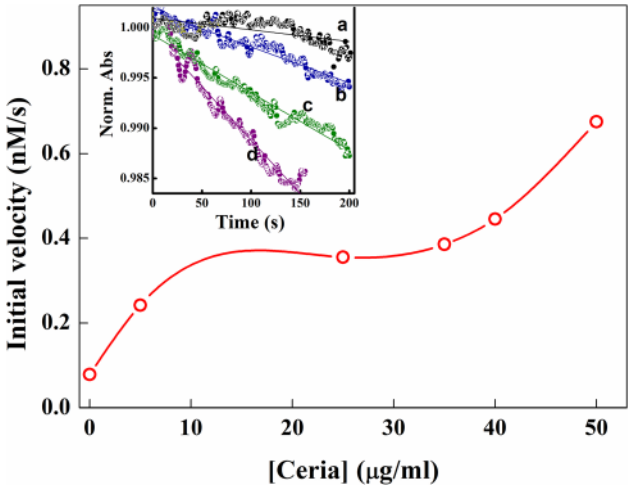


**Figure 5:** Peroxidase activity exhibited by different concentration of ceria nanoparticles. Inset shows the time dependent peroxidase-like activity for different concentration (a → d) of ceria nanoparticles.

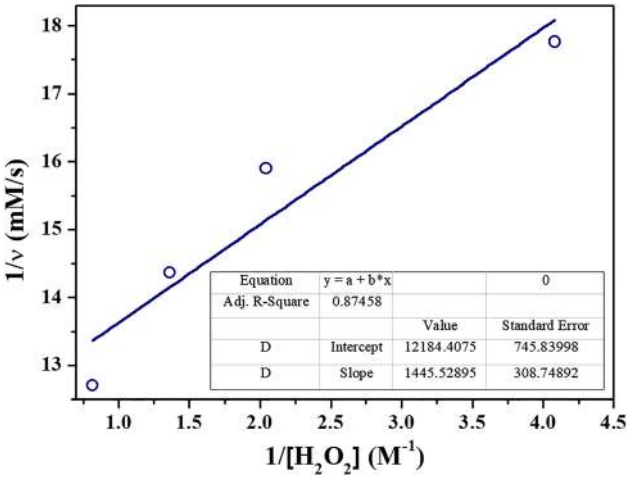


**Figure 7:** Double reciprocal plot of initial velocity for the decay of MG by $H_2O_2$ catalyzed by ceria nanoparticles as a function of hydrogen peroxide concentration.

affinity of ceria nanoparticles with $H_2O_2$, and higher affinity with MG.

## 4 Conclusions

In our previous work, ceria nanoparticles embedded in the Psf membrane matrix, exhibited the enhanced radiation resistant (up to 500 kGy of γ-radiation dose) properties and improved lifetime around five times as compared to the control Psf membrane. One of the probabilities for the enhanced stability is the scavenging of ROS generated during the radiolysis of water by ceria nanoparticles. In this work, the underlying mechanism and kinetics of ceria nanoparticle to scavenge the highly reactive free radicals was investigated. The $^{\bullet}OH$ radical scavenging of Ceria nanoparticles as evaluated from the inhibition of MG degradation showed that increasing ceria concentration showed higher $^{\bullet}OH$ radical scavenging. The peroxidase like activity of ceria nanoparticles was evaluated and the maximum initial velocity was found to increase gradually with the loading of ceria from 0.418 nM/s (blank MG) to 0.676 nM/s (for 1-Ce MMMs, 1% ceria loading in MMMs). The presence of both $Ce^{3+}$ and $Ce^{4+}$ ionic states of cerium in the ceria nanoparticles provided them the ability to scavenge hydroxyl radicals and $H_2O_2$. The distinctive scavenging capability of free radicals by ceria provides significant opportunities to the Psf-ceria MMMs for application in the γ-radiation environment.

**Author contributions:** All the authors have accepted responsibility for the entire content of this submitted manuscript and approved submission.
**Research funding:** None declared.
**Conflict of interest statement:** The authors declare no conflicts of interest regarding this article.

## References

Anandkumar, M., C. H. Ramamurthy, C. Thirunavukkarasu, and K. S. Babu. 2015. "Influence of Age on the Free-Radical Scavenging Ability of CeO2 and Au/CeO2 Nanoparticles." *Journal of Materials Science* 50: 2522–31.

Babu, S., A. Velez, K. Wozniak, J. Szydlowska, and S. Seal. 2007. "Electron Paramagnetic Study on Radical Scavenging Properties of Ceria Nanoparticles." *Chemical Physics Letters* 442: 405–8.

Bedar, A., R. K. Lenka, N. Goswami, V. Kumar, A. K. Debnath, D. Sen, S. Kumar, S. Ghodke, P. K. Tewari, R. C. Bindal, and S. Kar. 2019. "Polysulfone–Ceria Mixed-Matrix Membrane with Enhanced Radiation Resistance Behavior." *ACS Applied Polymer Materials* 1: 1854–65.

Bedar, A., P. K. Tewari, R. C. Bindal, and S. Kar. 2020. "Enhancing γ-radiation Resistant Property of Polysulfone Membranes with Carboxylated Nanodiamond: Impact and Effect of Surface Tunability." *Applied Surface Science* 507: 144897.

Beie, H.-J., and A. Gnörich. 1991. "Oxygen Gas Sensors Based on CeO2 Thick and Thin Films." *Sensors and Actuators B: Chemical* 4: 393–9.

Belkhir, N., D. Bouzid, and V. Herold. 2009. "Wear Behavior of the Abrasive Grains Used in Optical Glass Polishing." *Journal of Materials Processing Technology* 209: 6140–5.

Bosnjakovic, A., and S. Schlick. 2004. "Nafion Perfluorinated Membranes Treated in Fenton Media: Radical Species Detected by ESR Spectroscopy." *The Journal of Physical Chemistry B* 108: 4332–7.

Bouzigues, C., T. Gacoin, and A. Alexandrou. 2011. "Biological Applications of Rare-Earth Based Nanoparticles." *ACS Nano* 5: 8488–505.

Brown, J., and J. O'Donnell. 1975. "Effects of Gamma Radiation on Two Aromatic Polysulfones." *Journal of Applied Polymer Science* 19: 405–17.

Cafun, J.-D., K. O. Kvashnina, E. Casals, V. F. Puntes, and P. Glatzel. 2013. "Absence of Ce3+ Sites in Chemically Active Colloidal Ceria Nanoparticles." *ACS Nano* 7: 10726–32.

Campbell, C. T., and C. H. Peden. 2005. "Oxygen Vacancies and Catalysis on Ceria Surfaces." *Science* 309: 713–14.

Celardo, I., J. Z. Pedersen, E. Traversa, and L. Ghibelli. 2011. "Pharmacological Potential of Cerium Oxide Nanoparticles." *Nanoscale* 3: 1411–20.

Challenger, O., J. Braven, D. Harwood, K. Rosen, and G. Richardson. 1996. "Negative Air Ionisation and the Generation of Hydrogen Peroxide." *The Science of the Total Environment* 177: 215–19.

Conesa, J 1995. "Computer Modeling of Surfaces and Defects on Cerium Dioxide." *Surface Science* 339: 337–52.

Corma, A., P. Atienzar, H. Garcia, and J.-Y. Chane-Ching. 2004. "Hierarchically Mesostructured Doped CeO2 with Potential for Solar-Cell Use." *Nature Materials* 3: 394.

Esch, F., S. Fabris, L. Zhou, T. Montini, C. Africh, P. Fornasiero, G. Comelli, and R. Rosei. 2005. "Electron Localization Determines Defect Formation on Ceria Substrates." *Science* 309: 752–5.

Fernandez-Garcia, S., L. Jiang, M. Tinoco, A. B. Hungria, J. Han, G. Blanco, J. J. Calvino, and X. Chen. 2016. "Enhanced Hydroxyl Radical Scavenging Activity by Doping Lanthanum in Ceria Nanocubes." *The Journal of Physical Chemistry C* 120: 1891–901.

Goris, B., S. Turner, S. Bals, and G. Van Tendeloo. 2014. "Three-dimensional Valency Mapping in Ceria Nanocrystals." *ACS Nano* 8: 10878–84.

Hegazy, E.-S. A., T. Sasuga, M. Nishii, and T. Seguchi. 1992. "Irradiation Effects on Aromatic Polymers: 1. Gas Evolution by Gamma Irradiation." *Polymer* 33: 2897–903.

Hu, Z., S. Haneklaus, G. Sparovek, and E. Schnug. 2006. *Rare Earth Elements in Soils* 37, https://doi.org/10.1080/00103620600628680.

Izu, N., W. Shin, and N. Murayama. 2003. "Fast Response of Resistive-type Oxygen Gas Sensors Based on Nano-Sized Ceria Powder." *Sensors and Actuators B: Chemical* 93: 449–53.

Jasinski, P., T. Suzuki, and H. U. Anderson. 2003. "Nanocrystalline Undoped Ceria Oxygen Sensor." *Sensors and Actuators B: Chemical* 95: 73–7.

Kašpar, J., P. Fornasiero, and M. Graziani. 1999. "Use of CeO 2-based Oxides in the Three-Way Catalysis." *Catalysis Today* 50: 285–98.

Li, H.-Y., H. F. Wang, X. O Gong, Y. L. Guo, Y. Guo, G. Lu, and P. Hu. 2009. "Multiple Configurations of the Two Excess 4 F Electrons on Defective CeO 2 (111): Origin and Implications." *Physical Review B* 79: 193401.

Liu, X., D. Huang, C. Lai, L. Qin, G. Zeng, P. Xu, B. Li, H. Yi, and M. Zhang. 2019. "Peroxidase-Like Activity of Smart Nanomaterials and Their Advanced Application in Colorimetric Glucose Biosensors." *Small* 15: 1900133.

Mu, J., Y. Wang, M. Zhao, and L. Zhang. 2012. "Intrinsic Peroxidase-like Activity and Catalase-like Activity of Co 3 O 4 Nanoparticles." *Chemical Communications* 48: 2540–2.

Mu, J., J. Li, X. Zhao, E.-C. Yang, and X.-J. Zhao. 2018. "Novel Urchin-like Co9S8 Nanomaterials with Efficient Intrinsic Peroxidase-like Activity for Colorimetric Sensing of Copper (II) Ion." *Sensors and Actuators B: Chemical* 258: 32–41.

Mullins, D. R. 2015. "The Surface Chemistry of Cerium Oxide." *Surface Science Reports* 70: 42–85.

Murakami, K., and H. Kudo. 2007. "Gamma-rays Irradiation Effects on Polysulfone at High Temperature." *Nuclear Instruments and Methods in Physics Research Section B: Beam Interactions with Materials and Atoms* 265: 125–9.

Ng, L. Y., A. W. Mohammad, C. P. Leo, and N. Hilal. 2013. "Polymeric Membranes Incorporated with Metal/metal Oxide Nanoparticles: a Comprehensive Review." *Desalination* 308: 15–33.

Patil, S., S. Kuiry, S. Seal, and R. Vanfleet. 2002. "Synthesis of Nanocrystalline Ceria Particles for High Temperature Oxidation Resistant Coating." *Journal of Nanoparticle Research* 4: 433–8.

Rupiasih, N. N., and P. Vidyasagar. 2008. "Comparative Study of Effect of Low and Medium Dose Rate of γ Irradiation on Microporous Polysulfone Membrane Using Spectroscopic and Imaging Techniques." *Polymer Degradation and Stability* 93: 1300–7.

Schadler, L. S. 2018. *6.3 The Elusive Interphase/Interface in Polymer Nanocomposites*. Elsevier.

Schlick, S., M. Danilczuk, A. R. Drews, and R. S. Kukreja. 2016. "Scavenging of Hydroxyl Radicals by Ceria Nanoparticles: Effect of Particle Size and Concentration." *The Journal of Physical Chemistry C* 120: 6885–90.

Stambouli, A. B., and E. Traversa. 2002. "Solid Oxide Fuel Cells (SOFCs): a Review of an Environmentally Clean and Efficient Source of Energy." *Renewable and Sustainable Energy Reviews* 6: 433–55.

Stefanik, T. S., and H. L. Tuller. 2001. "Ceria-based Gas Sensors." *Journal of the European Ceramic Society* 21: 1967–70.

Trovarelli, A. 1996. "Catalytic Properties of Ceria and CeO2-Containing Materials." *Catalysis Reviews* 38: 439–520.

Vinothkumar, G., S. Rengaraj, P. Arunkumar, S. W. Cha, and K. Suresh Babu. 2018. "Ionic Radii and Concentration Dependency of RE3+ (Eu3+, Nd3+, Pr3+, and La3+)-Doped Cerium Oxide Nanoparticles for Enhanced Multienzyme-Mimetic and Hydroxyl Radical Scavenging Activity." *The Journal of Physical Chemistry C* 123: 541–53.

Wang, L., K. Zhang, Z. Song, and S. Feng. 2007. "Ceria Concentration Effect on Chemical Mechanical Polishing of Optical Glass." *Applied Surface Science* 253: 4951–4.

Wang, Y.-J., H. Dong, G. M. Lyu, H. Y. Zhang, J. Ke, L. Q. Kang, J. L. Teng, L. D. Sun, R. Si, J. Zhang, and Y. J. Liu. 2015. "Engineering the Defect State and Reducibility of Ceria Based Nanoparticles for Improved Anti-oxidation Performance." *Nanoscale* 7: 13981–90.

Wu, H., F. Li, S. Wang, J. Lu, J. Li, Y. Du, X. Sun, X. Chen, J. Gao, and D. Ling. 2018. "Ceria Nanocrystals Decorated Mesoporous Silica Nanoparticle Based ROS-Scavenging Tissue Adhesive for Highly Efficient Regenerative Wound Healing." *Biomaterials* 151: 66–77.

Xu, C., and X. Qu. 2014. "Cerium Oxide Nanoparticle: a Remarkably Versatile Rare Earth Nanomaterial for Biological Applications." *NPG Asia Materials* 6: e90.

Yang, S., and L. Gao. 2006. "Controlled Synthesis and Self-Assembly of CeO2 Nanocubes." *Journal of the American Chemical Society* 128: 9330–1.

Zhang, F., Q. Jin, and S.-W. Chan. 2004. "Ceria Nanoparticles: Size, Size Distribution, and Shape." *Journal of Applied Physics* 95: 4319–26.

Zhao, H., Y. Dong, P. Jiang, G. Wang, and J. Zhang. 2015. "Highly Dispersed CeO2 on TiO2 Nanotube: a Synergistic Nanocomposite with Superior Peroxidase-like Activity." *ACS applied materials & interfaces* 7: 6451–61.

Zhang, D.-Y., H. Liu, C. Li, M. R. Younis, S. Lei, C. Yang, J. Lin, Z. Li, and P. Huang. 2020. "Ceria Nanozymes with Preferential Renal Uptake for Acute Kidney Injury Alleviation." *ACS Applied Materials & Interfaces* 12 (51): 56830–8.